

1 **Target cell adhesion limits macrophage phagocytosis and promotes**
2 **trogocytosis**

3

4 Kirstin Rollins¹, Sareen Fiaz¹, Meghan Morrissey^{1, *}

5

6

7 ¹Molecular Cellular and Developmental Biology Department, University of California,
8 Santa Barbara, Santa Barbara CA

9

10 *Lead contact morrissey@ucsb.edu

11

12 Keywords: macrophage, phagocytosis, trogocytosis, CAR (chimeric antigen receptor).

13 Fc Receptor, IgG, CD47

14 **Abstract:**

15 Macrophage phagocytosis is an essential immune response that eliminates pathogens,
16 antibody-opsonized cancer cells and debris. Macrophages can also trogocytose, or nibble,
17 targets. Trogocytosis and phagocytosis are often activated by the same signal, including IgG
18 antibodies. What makes a macrophage trogocytose instead of phagocytose is not clear. Using
19 both CD47 antibodies and a Her2 Chimeric Antigen Receptor (CAR) to induce phagocytosis, we
20 found that macrophages preferentially trogocytose adherent target cells instead of phagocytose
21 in both 2D cell monolayers and 3D cancer spheroid models. Disrupting target cell integrin using
22 an RGD peptide or through CRISPR-Cas9 knockout of the α V integrin subunit in target cells
23 increased macrophage phagocytosis. Conversely, increasing cell adhesion by ectopically
24 expressing E-Cadherin in Raji B cell targets reduced phagocytosis. Finally, we examined
25 phagocytosis of mitotic cells, a naturally occurring example of cells with reduced adhesion.
26 Arresting target cells in mitosis significantly increased phagocytosis. Together, our data show
27 that target cell adhesion limits phagocytosis and promotes trogocytosis.

28

29

30

31 **Introduction**

32 Macrophages are innate immune cells that surveille the body for signs of injury or
33 infection. Macrophages clear diverse targets, including pathogens, dying cells and debris,
34 through phagocytosis (Freeman & Grinstein, 2021). Phagocytosis is critical for maintaining
35 tissue homeostasis, protecting against infection and preventing autoimmunity (Gordon, 2016).
36 Macrophages are also key effectors of many cancer therapies (Guerriero, 2018; Van Wagoner
37 et al., 2023; Weiskopf & Weissman, 2015). Therapeutic antibodies like rituximab (CD20
38 antibody) and trazituzumab (Her2 antibody) bind to cancer cells and signal for macrophage
39 uptake (Chao et al., 2010; Gül et al., 2014; Manches et al., 2003; Shi et al., 2015; Uchida et al.,
40 2004; Weiskopf & Weissman, 2015). IgG is recognized by the Fc Receptor in macrophages
41 (Nimmerjahn & Ravetch, 2008). Even many antibodies originally designed to block the function
42 of their target benefit from activating the Fc Receptor (Chen et al., 2019; Dahan et al., 2016).
43 More recently, engineering macrophages to express synthetic Chimeric Antigen Receptors
44 (CARs) that trigger phagocytosis has been shown to shrink tumors in mouse models (Klichinsky
45 et al., 2020; Morrissey et al., 2018; Sloas et al., 2021).

46 Activating phagocytosis of cancer cells is particularly exciting in solid tumors (Sloas et
47 al., 2021). Macrophages are one of the most prevalent immune infiltrates of the solid tumor
48 microenvironment (de Visser & Joyce, 2023). However, most studies on the mechanism of
49 phagocytosis use suspended targets, including apoptotic cells, blood cancer cell lines, and
50 reconstituted particles (Arandjelovic & Ravichandran, 2015; Gül et al., 2014; Joffe et al., 2020;
51 Morrissey et al., 2018). Unlike these models, solid tumors have complex cell-cell and cell-ECM
52 interactions that adhere cancer cells to the surrounding environment. How macrophages
53 phagocytose a cell incorporated into a 3D tissue is not clear.

54 Phagocytosis of adherent targets often requires additional steps to remove the target
55 from its environment. Adherent bacteria are pried from their substrate by a macrophage “hook-
56 and-shovel” mechanism, wherein macrophages wedge lamellipodia between the bacteria and

57 substrate to destroy adhesion molecules (Möller et al., 2013). Dying cells are loosened from
58 their neighbors as focal adhesion and cell-cell contacts are dismantled during apoptosis
59 (Brancolini et al., 1997). In melanoma models, macrophages cluster to cooperatively remove
60 cancer cells (Dooling et al., 2023, 2024). These studies suggest that cell-cell and cell-substrate
61 adhesion is a barrier to phagocytosis.

62 In addition to phagocytosis, macrophages can trogocytose, or nibble, target cells
63 (Bettadapur et al., 2020). Trogocytosis has been observed in diverse contexts, including
64 immune cell communication, developmental remodeling, and parasitic attack (Abdu et al., 2016;
65 Gao et al., 2024; Hudrisier et al., 2001; Joly & Hudrisier, 2003; Mercer et al., 2018; Ralston et
66 al., 2014; Weinhard et al., 2018). Trogocytosis and phagocytosis are triggered by the same
67 signals, including IgG antibodies, and share many molecular regulators (Bettadapur et al., 2020;
68 Lindorfer & Taylor, 2022). What makes a macrophage trogocytose instead of phagocytose is not
69 clear.

70 Macrophages also trogocytose antibody opsonized cancer cells during cancer therapy
71 (Beum et al., 2011; Lindorfer & Taylor, 2022; Park et al., 2022; Velmurugan et al., 2016).
72 Trogocytosis of antibody opsonized cancer cells can lead to cancer cell death (Finotti et al.,
73 2023; Matlung et al., 2018; Velmurugan et al., 2016). However, trogocytosis is also associated
74 with ‘antigen shaving’, or the removal of target antigens, which limits antibody efficacy by
75 making cancer cells more difficult for the immune system to detect (Beum et al., 2011; Hamieh
76 et al., 2019; Kennedy et al., 2004; Williams et al., 2006). Biasing therapies towards
77 phagocytosis could potentially improve cancer cell clearance (Williams et al., 2006; Zent et al.,
78 2014).

79 In this study, we investigated how target cell adhesion impacts macrophage
80 phagocytosis. We used an ovarian cancer cell line in 2D monolayers or 3D spheroids as a
81 phagocytic target. Macrophages preferentially trogocytosed (nibbled) adherent cells and
82 phagocytosed suspended cells. We show that this preference for trogocytosis was reversed if

83 we reduced or eliminated cell-substrate adhesion. We also show that suspended cells were
84 primarily trogocytosed instead of phagocytosed if we increased cell-cell adhesion. Finally, we
85 observed that mitotic cells were more susceptible to phagocytosis than cells in interphase,
86 indicating that macrophages may capitalize on opportune moments for phagocytosis upon the
87 disassembly of adhesion. Together our results demonstrate that the macrophages preferentially
88 trogocytose adherent targets.

89 **Results**

90

91 **Construction of a Her2-targeting Chimeric Antigen Receptor**

92 To study how macrophages attack adherent cells, we selected the SKOV3 ovarian
93 cancer cell line as our target cell. This cell line has high expression of the human epidermal
94 growth hormone receptor 2 (Her2/ErbB2). Trastuzumab, an antibody targeting Her2, is a
95 common cancer therapy and has previously been shown to induce cancer cell internalization
96 (Petricevic et al., 2013; Shi et al., 2015; Velmurugan et al., 2016). Her2-targeting CAR
97 macrophages are being investigated in clinical trials (Klichinsky et al., 2020; Sloas et al., 2021).

98 We elected to induce phagocytosis with a Her2-targeted CAR, since Her2 antibodies
99 inhibit Her2 signaling in addition to activating phagocytosis (Hudziak et al., 1989; Swain et al.,
100 2023). We designed a Her2-targeting CAR comprised of an extracellular Her2 antibody
101 fragment (scFv from 4D5-8 (Carter et al., 1992)), the CD8 hinge and transmembrane domain
102 from successful CAR T molecules (Fesnak et al., 2016; Kochenderfer et al., 2009), the
103 intracellular signaling domain from the mouse Fc Receptor common gamma chain (Kern et al.,
104 2021; Morrissey et al., 2018), and a GFP tag (Fig. 1A). A similar Her2 CAR was recently shown
105 to decrease cancer growth in mouse xenograft models lacking T cells, suggesting that Her2
106 CAR macrophages can shrink tumors without engaging the adaptive immune system (Klichinsky
107 et al., 2020).

108 To test whether the Her2 CAR could stimulate macrophage activity, we incubated Her2
109 CAR GFP or control GFP macrophages with Her2+ SKOV3 ovarian cancer cells dyed in Far
110 Red Cell Trace. After 2 hours, we measured the cancer cell uptake via flow cytometry. We
111 found that Her2 CAR expression increased macrophage internalization of SKOV3 cells (Fig.
112 1B).

113

114 **Her2 CAR macrophages primarily trogocytose target cells**

115 To further characterize macrophage activity against adherent targets, we used confocal
116 live-cell timelapse imaging of Her2 CAR macrophage and SKOV3 co-incubations. SKOV3 cells
117 were infected with a membrane tethered mCherry (mCherry-CAAX). To our surprise,
118 phagocytosis of cancer cells was relatively rare. We observed that only 10% of macrophages
119 phagocytosed during our 10 hour timelapse (Fig. 1C, Video 1). In contrast, 95% of
120 macrophages trogocytosed, or nibbled, the cancer cell membrane (Fig. 1C, Video 2). This data
121 shows that most SKOV3 internalization is trogocytosis, rather than phagocytosis.

122

123 **Her2 CAR macrophages limit the growth of SKOV3 spheroids**

124 Our previous experiments in monolayers lacked the 3D architecture and cell-to-cell
125 adhesion normally found in a solid tumor. To investigate macrophage eating dynamics in a
126 simple 3D tissue model, we built spheroids of SKOV3 cells. To generate spheroids, we plated
127 membrane labeled (mCh-CAAX) SKOV3 cells in a low adhesion dish in media supplemented
128 with 2.5% matrigel to favor cell-cell interactions (Ivascu & Kubbies, 2007; Heredia-Soto et al.,
129 2018; Tofani et al., 2020). By 72 hours, the SKOV3 cells assembled into consistent, compact
130 spheroids ($445 \pm 65 \mu\text{m}$ in diameter). We then transferred the pre-assembled SKOV3 spheroids
131 into a matrigel dome containing Her2 CAR or control GFP macrophages. Z-stack images
132 showed that both GFP and Her2 CAR macrophage could invade into the spheroids within 24
133 hours (Videos 3,4). We tracked spheroid size for 10 days via spinning disc confocal imaging
134 (Fig. 2A,B). We found that Her2 CAR macrophages significantly reduced the size of the
135 spheroids compared to no macrophages or GFP macrophages (Fig. 2B). In the final timepoints,
136 a large portion of the remaining mCherry signal appeared to be from macrophages that had
137 internalized cancer cells (Fig. 2C). This demonstrates that Her2 CAR macrophages effectively
138 attack 3D cancer spheroids.

139

140 **Macrophages trogocytose more than phagocytose in a 3D environment**

141 We next sought to determine if macrophages attack SKOV3 spheroids via trogocytosis
142 as in the 2D culture system. Brief timelapse imaging revealed several examples of trogocytosis
143 and phagocytosis but was difficult to quantify (Video 5, Fig. S1). Instead, we double-labeled
144 cancer cells with a membrane tethered mCherry (mCh-CAAX) and a nuclear iRFP (H2B-iRFP;
145 Fig. 2D). If a cancer cell were phagocytosed, both nuclear and membrane signals would be
146 detected within the macrophage, confirming whole cell engulfment. If a cancer cell were
147 trogocytosed, only the membrane signal would be detected within the macrophage. We imaged
148 the spheroids daily for 10 days and quantified the fraction of macrophages that had internalized
149 mCherry (trogocytosed) or iRFP and mCherry (phagocytosed) (Fig. 2D,E). We found that
150 trogocytosis was more common than phagocytosis in 3D spheroid models (Fig. 2E), as in the
151 2D culture system. Trogocytic macrophages were clearly observed in the first days after
152 macrophage infiltration, while phagocytic macrophages slowly accumulated over time (Fig. 2E).

153

154 **Macrophage trogocytosis strips the antigen from target cells**

155 Several clinical studies have noted that trogocytosis of antibody-opsonized cancer cells
156 removes target antigen from the cancer cell surface in vivo (Hamieh et al., 2019; Lindorfer &
157 Taylor, 2022; Park et al., 2022; Williams et al., 2006). This process, known as antigen shaving,
158 makes the cancer cells more difficult for immune cells to detect (Hamieh et al., 2019; Lindorfer &
159 Taylor, 2022; Williams et al., 2006). We checked for antigen shaving by immunostaining for
160 Her2 on SKOV3 cells after macrophage treatment. We found that treatment with Her2 CAR
161 macrophages led to a substantial decrease in the surface levels of Her2, whereas GFP
162 macrophages did not change Her2 surface levels (Fig. 3A,B). Overall, this data illustrates the
163 high level of trogocytosis in our system.

164

165 **Macrophages primarily phagocytose suspended cells and trogocytose adherent cells**

166 Prior studies using antibody opsonized B cells have reported high levels of phagocytosis
167 (for example, (Chao et al., 2010; Gül et al., 2014)). We have previously seen that CD19 CAR
168 macrophages targeting B cells phagocytose many cancer cells during a similar timelapse
169 microscopy experiment (Mishra et al., 2023; Morrissey et al., 2018). We hypothesized that
170 adherent cells may be more difficult to phagocytose and more likely to be trogocytosed than
171 suspended cells. To see if this was broadly true for multiple adherent cell lines, we assembled a
172 panel of cancer cell lines, including three adherent cell lines and two suspension cell lines. We
173 expressed membrane tethered mCherry-CAAX and a nuclear H2B-iRFP marker in all the cell
174 lines, opsonized the cells with a CD47 antibody, and measured trogocytosis and phagocytosis
175 with flow cytometry (Fig. 4A). The selected cancer cell lines expressed a reasonably uniform
176 level of CD47, a ‘Don’t Eat Me’ signal (Fig. S2). CD47 antibodies trigger phagocytosis by
177 blocking the inhibitory CD47 signal and engaging with macrophage Fc Receptors through the
178 antibody Fc domain (Chao et al., 2010; Jaiswal et al., 2009; Majeti et al., 2009; Osorio et al.,
179 2023). We found that the total number of macrophages internalizing any cancer cell material
180 (mCherry positive) was relatively uniform across the five cell lines (Fig. 4B). Strikingly, we
181 observed that the suspended cell lines were primarily phagocytosed (60-70% of total activity)
182 and the adherent cell lines were primarily trogocytosed (80-90% of total activity; Fig. 4C). Since
183 antibody opsonization induced trogocytosis of multiple adherent cell lines, this demonstrates
184 that trogocytosis is not a unique feature of the SKOV3 target cell, or of the CAR macrophage
185 system.

186

187 **Decreasing target cell adhesion increases phagocytosis**

188 We hypothesized that decreasing target cell adhesion could shift macrophage behavior
189 from trogocytosis to phagocytosis. First, we tested if detaching SKOV3 cells from a substrate
190 increased phagocytosis. We compared phagocytosis of adherent SKOV3 cells to phagocytosis

191 of detached SKOV3 cells. Using timelapse microscopy to measure phagocytosis, we found
192 Her2 CAR macrophages phagocytosed more SKOV3 cells when the cells were presented in
193 suspension than when allowed to adhere to a tissue culture plate (Fig. 5A, Fig. S3). This was
194 true whether the macrophages were mixed with the SKOV3 cells in suspension, or pre-adhered
195 to the tissue culture plate (Fig. S3). Control GFP macrophages did not phagocytose more
196 suspended cells, suggesting this increase in phagocytosis was due to Her2 CAR activity not
197 increased cell death (Fig. 5A). Together, these data show that suspended cells are more readily
198 phagocytosed than adherent cells.

199 We next sought to modulate cell-substrate attachment by decreasing integrin adhesion.
200 To weaken cell-substrate adhesion, we treated SKOV3 cells expressing membrane tethered
201 mCherry and nuclear iRFP with the RGD peptide, Cilengitide Trifluoroacetate. This RGD
202 peptide primarily inhibits the integrins $\alpha_v\beta_3$ and $\alpha_v\beta_5$ (Dechantsreiter et al., 1999). We verified
203 that the RGD peptide caused the SKOV3 cells to adopt a rounded morphology and decreased
204 surface area characteristic of lowered adhesion, although the cells were not completely
205 suspended (Fig. 5B). To minimize the RGD peptide's effect on the macrophages, we washed
206 out the RGD peptide before adding Her2 CAR or control GFP macrophages. We then measured
207 phagocytosis and trogocytosis by live-cell timelapse microscopy. We found that RGD peptide
208 promoted phagocytosis and reduced trogocytosis, although fewer cells were phagocytosed than
209 when the SKOV3 cells were fully detached from the substrate (Fig. 5A). Again, control GFP
210 macrophages did not phagocytose additional target cells in the RGD condition, suggesting that
211 these cells are not exposing additional pro-phagocytic signals. This suggests that inhibiting
212 integrin is sufficient to increase phagocytosis.

213 To confirm that inhibiting integrin in the target cell increases phagocytosis, we used
214 CRISPR-Cas9 to knock out specific integrin subunits in SKOV3 cells (Fig. S4, Table S1). We
215 selected integrin β_1 and β_5 (ITGB1, ITGB5) as dysregulation of these receptors is associated
216 with cancer development and progression in a wide variety of solid tumors, including Her2+

217 breast and ovarian cancers (Casey et al., 2001; Davidson et al., 2003; Desgrosellier & Cheresch,
218 2010). We also selected integrin α V (ITGAV) as it is reported to affect ovarian cancer
219 proliferation and metastasis (Casey et al., 2001; Cruet-Hennequart et al., 2003; Davidson et al.,
220 2003). ITGAV knockout target cells were phagocytosed more than control cells (Fig. 5C). ITGB1
221 and ITGB5 knockouts did not significantly impact phagocytosis, which could indicate
222 redundancy since ITGAV pairs with both B subunits. These findings demonstrate decreasing
223 cell-substrate adhesion promotes phagocytosis.

224

225 **Increasing cell-cell adhesion in suspension cells decreases phagocytosis**

226 We next wondered if we could conversely increase adhesion to limit phagocytosis. We
227 overexpressed E-Cadherin (CDH1) in Raji B cells, a suspension cell line. Raji B cells expressing
228 E-Cadherin formed multicellular clusters, indicating increased cell-cell adhesion (Fig. 6A). We
229 opsonized wild type and E cadherin overexpressing Rajis with a mouse anti-human CD47
230 antibody to induce phagocytosis. Macrophages with Rajis expressing either iRFP-CAAX or
231 H2B-iRFP were co-incubated for 2 hours before dissociating the clustered conditions into a
232 single-cell solution for flow cytometry. The level of phagocytosis (H2B-iRFP internalization) was
233 significantly lower in the E-Cadherin overexpressing clusters than the wild type Raji cells (Fig.
234 6B). In contrast, the fraction of macrophages with internalized Raji cell membrane (iRFP-CAAX),
235 either by trogocytosis or phagocytosis, did not change (Fig. 6C). This suggests that
236 macrophages encountered a similar number of Raji targets, but did not phagocytose the E
237 cadherin overexpressing cells. Overall, this demonstrates that increasing cell-cell adhesion in
238 target cells limits phagocytosis.

239

240 **Dividing cells are more vulnerable to phagocytic attack**

241 Our data demonstrates that macrophages phagocytose cellular targets with weakened
242 attachment to substrates and neighboring cells. However, even without any synthetic

243 manipulations of target cell adhesion, we observed that 10% of macrophages could
244 phagocytose adherent SKOV3 cells (Fig. 1E). We revisited these intrinsic phagocytic attacks in
245 our timelapses and found that a large number of the phagocytosed cells appeared to be in the
246 process of cell division (Fig. 7A, Video 6). While only 4% of SKOV3 cells were dividing at any
247 time, 38% of the phagocytosed SKOV3 cells were undergoing division (Fig. 7B). Mitotic cells are
248 known to have reduced adhesion (Akhmanova et al., 2022; Dix et al., 2018; Lock et al., 2018;
249 Marchesi et al., 2014), so this observation is consistent with our overall hypothesis that reduced
250 cell adhesion promotes phagocytosis.

251 To examine this more closely, we generated a SKOV3 cell line expressing Fluorescent
252 Ubiquitination-based Cell Cycle Indicator (FUCCI) to read out the stage of the cell cycle. The
253 FUCCI reporter consists of an mCherry tagged hGeminin that will accumulate in S/G2/M before
254 being degraded, and a BFP tagged hCdt1 will be detected in G1 (Fig. 7C)(Sakaue-Sawano et
255 al., 2008; Sato et al., 2019). Using this reporter, we found that 94% of phagocytosed SKOV3
256 were mCherry positive, indicating that these cells were in S/G2/M, while only 53% percent of the
257 overall SKOV3 population was mCherry positive (Fig. 7D). This is consistent with our
258 observation that SKOV3 cells are more likely to be phagocytosed while dividing.

259 We next hypothesized that arresting target cells in mitosis would increase phagocytosis.
260 To test this, we treated cancer cells with paclitaxel (Taxol) or S-trityl-cysteine (STLC). Paclitaxel
261 is a cancer chemotherapeutic that inhibits microtubule disassembly, and prevents cells from
262 passing the spindle assembly checkpoint (Horwitz, 1994). STLC inhibits Eg5, a mitotic kinesin
263 necessary for assembly of the bipolar spindle, locking the cells in prometaphase (Skoufias et al.,
264 2006). After 20 hours of paclitaxel and STLC treatment, nearly all FUCCI SKOV3 cells were
265 mCherry positive indicating cell cycle arrest (Fig. 7C,D). The mitotic arrest did not induce
266 apoptosis by 20 hours, as we did not detect an increase in phosphatidylserine exposure (Fig.
267 S5). We then co-incubated the arrested cells with Her2 CAR macrophages and measured
268 phagocytosis by timelapse microscopy. We found that cancer cells arrested in mitosis were

269 phagocytosed significantly more than untreated controls (Fig. 5E). This data suggests that
270 mitotic cells are easier to phagocytose than interphase cells.

271

272

273 **Discussion**

274

275 While many antibody therapies and CAR macrophages are presumed to primarily trigger
276 phagocytosis, we have found that phagocytosis of adherent cells is relatively rare. Instead,
277 macrophages trogocytose, or nibble, these cells. Reducing target cell adhesion by disrupting
278 integrin increased macrophage phagocytosis and reduced trogocytosis. Conversely, increasing
279 cell-cell adhesion in a suspended cell line reduced phagocytosis. Overall, this data shows that
280 target cell adhesion regulates phagocytosis and trogocytosis.

281 Very little is known about what makes a macrophage trogocytose instead of
282 phagocytose. Trogocytosis and phagocytosis are controlled by nearly identical signaling
283 pathways in the macrophage (Bettadapur et al., 2020). Trogocytosis and phagocytosis also
284 occur on diverse targets, making it unlikely that there is a specific molecule that signals for
285 trogocytosis instead of phagocytosis (Bettadapur et al., 2020). Instead, the biophysical
286 properties of the target cell may guide the macrophage to trogocytose instead of phagocytose.
287 A recent study found that target membrane tension is a key regulator of trogocytosis (Cornell et
288 al., 2024). Lower membrane tension increased trogocytosis, while higher membrane tension
289 favored phagocytosis. Our study also supports the hypothesis that the target's biophysical
290 properties determine if a macrophage performs phagocytosis or trogocytosis.

291 Trogocytosis has been observed in many clinical settings (Hamieh et al., 2019; Lindorfer
292 & Taylor, 2022; Park et al., 2022; Williams et al., 2006). The impact of trogocytosis is murky.
293 Sometimes, trogocytosis kills the target cell (Finotti et al., 2023; Matlung et al., 2018; Park et al.,
294 2022; Velmurugan et al., 2016). In other cases, trogocytosis limits the efficacy of cancer

295 therapy. Trogocytosis of the CD20 antibody therapy rituximab causes a significant reduction in
296 CD20 levels on cancer cells in rituximab-treated patients (Kennedy et al., 2004). Optimizing the
297 rituximab dosing schedule to limit trogocytosis improved efficacy (Williams et al., 2006; Zent et
298 al., 2014). Similarly, high affinity CAR T cells trogocytose target antigen from cancer cell's
299 surface leading to antigen escape (Hamieh et al., 2019). Re-engineering the CAR T molecule to
300 have a lower affinity increased efficacy by reducing antigen shaving. These studies suggest that
301 biasing antibody therapies towards phagocytosis instead of trogocytosis could significantly
302 reduce antigen shaving and improve clinical efficacy.

303 We found that arresting cancer cells in mitosis increased CAR macrophage
304 phagocytosis. Dividing cells disassemble focal adhesion, while remaining loosely attached to
305 their underlying substrate (Dix et al., 2018). This lowered adhesion allows macrophages to
306 squeeze past dividing cells and infiltrate cell-dense tissue (Akhmanova et al., 2022). Dividing
307 cells undergo other cell shape changes that may promote phagocytosis, including cell rounding.
308 However, given our data showing that decreasing cell adhesion promotes phagocytosis, we
309 attribute at least part of the increased phagocytosis to decreased cell adhesion. Interestingly, a
310 combination of paclitaxel and Her2 monoclonal antibody is a highly effective treatment for Her2
311 positive breast cancers (Giordano et al., 2022). This suggests that the current therapy regimen
312 could already benefit from enhanced phagocytosis due to mitotic arrest.

313 We also demonstrate that reducing integrin-mediated adhesion in target cells increased
314 macrophage phagocytosis. Integrin inhibitors have previously been targeted in several clinical
315 trials (Desgrosellier & Cheresh, 2010). Unfortunately, many of these integrin inhibitors failed in
316 clinical trials due to lack of efficacy. Our work suggests that while these inhibitors were
317 ineffective as a monotherapy, they may synergize with antibody therapies that induce
318 phagocytosis.

319 In some cases, trogocytosis is reported to kill cancer cells. Why trogocytosis is
320 sometimes lethal and sometimes not is unclear. Several of the studies showing death after

321 trogocytosis induce trogocytosis with a Her2 antibody (Matlung et al., 2018; Velmurugan et al.,
322 2016). We find that trogocytosis by Her2 CAR macrophages dramatically decreases Her2. Our
323 study measured Her2 levels on viable cancer cells, suggesting that this reduction in Her2 did
324 not immediately kill the cancer cells. However, this reduction in Her2 likely decreases cancer
325 cell fitness since Her2 provides a powerful pro-growth signal to Her2+ cancers. Future studies
326 will need to address the impact of trogocytosis on cancer cell fitness.

327 Macrophages co-operate to phagocytose in solid tumor models (Dooling et al., 2023,
328 2024). Our studies support the idea that cell-cell and cell-matrix adhesions are too strong for a
329 single macrophage to overcome during phagocytosis (Dooling et al., 2023). We speculate that
330 trogocytosis could be a mechanism for macrophage cooperation by weakening target cells. Our
331 data shows higher occurrence of trogocytosis than phagocytosis in the initial days after
332 macrophages infiltrate the spheroid. The subsequent increase in phagocytosis is consistent with
333 cancer cells dying due to trogocytosis, then their corpses being phagocytosed, or with
334 trogocytosis enabling phagocytosis. Currently, there are no tools to specifically block
335 trogocytosis without impacting phagocytosis as well, since the molecules involved in
336 trogocytosis appear to also be required for phagocytosis. Future studies will need to test how
337 trogocytosis impacts phagocytosis and antibody efficacy.

338

339 **Figure legends**

340

341 **Figure 1: Her2 CAR macrophages trogocytose target SKOV3 cells**

342 (A) Schematic shows the design of the Her2 CAR (right) compared to the native Fc Receptor
343 (left). The Her2 CAR contains an extracellular scFv recognizing Her2, and activates
344 phagocytosis via the intracellular signaling domain from the endogenous Fc Receptor common
345 gamma chain. (B) Schematic (left) describes the assay quantified in the graph (right). Her2 CAR
346 GFP or control GFP (GFP-CAAX) bone marrow derived macrophages (BMDMs) were mixed
347 with SKOV3 cells dyed with CellTrace Far Red. Flow cytometry was used to measure the
348 percent of macrophages (GFP+) that internalized cancer cell material (Far Red+). (C) Her2 CAR
349 GFP (green) macrophages were visualized interacting with SKOV3 cancer cells (mCh-CAAX;
350 magenta) using timelapse confocal microscopy. Stills from the images are depicted on the left,
351 and the percent of macrophages engaging in trogocytosis (internalizing part of a cell) or
352 phagocytosis (internalizing a whole cell) is graphed to the right. These stills correspond to Video
353 1 (top) and Video 2 (bottom). In B and C, data was compared using a Students T test. N= 3
354 experiments with independently generated and infected BMDMs. In all graphs, bars represent
355 the mean \pm SEM. Data collected on the same day is annotated with the same shape point. *
356 denotes $p < 0.05$, **** denotes $p < 0.0005$. Scale bar denotes 20 μm .

357

358 **Figure 2: Her2 CAR macrophages trogocytose more than phagocytose in 3D spheroid**
359 **models.**

360 (A) SKOV3 cells (mCh-CAAX, magenta) were assembled into a 3D spheroid and embedded in
361 matrigel alone (top), with control GFP (green) macrophages (middle) or with Her2 CAR GFP
362 (green) macrophages (bottom). Images are maximum projections of spinning disc confocal z
363 stacks. Dashed line highlights the spheroid boundary. Scale bars denote 500 μm . On days 5
364 and 10, multiple images were stitched together to capture the entire spheroid in the no

365 macrophage and GFP macrophage conditions. Unstitched images are presented on a grey
366 background so the image scale is consistent. (B) Graph depicts spheroid growth over time for
367 the same conditions shown in (A). Individual spheroids were tracked for 10 days, and the
368 diameter was normalized to the starting diameter. The length and width of the spheroid were
369 measured on the max projection of confocal z-stacks and averaged to calculate spheroid
370 diameter. N=6 spheroids acquired in 4 independent experiments. (C) Inset from (A) shows that
371 mCherry signal on day 10 is mostly contained within Her2 CAR GFP (green) macrophages.
372 Arrowheads point to macrophages. Scale bars denote 20 μ m. (D) Top image shows the H2B-
373 iRFP (blue), mCherry-CAAX (magenta) SKOV3 cell line used to assemble spheroids. Images
374 show examples of Her2 CAR GFP (green) macrophages that have phagocytosed (middle,
375 internalized nuclei position is highlighted with yellow arrowhead) or trogocytosed (bottom, yellow
376 arrowhead) SKOV3 cells. Scale bars denote 20 μ m. (E) The percent of Her2 CAR GFP
377 macrophages that had phagocytosed (internalized H2B-iRFP) or trogocytosed (internalized
378 mCh-CAAX) was quantified on each day. Only macrophages touching the spheroid were
379 included in the analysis. N= 3 spheroids from 3 independent experiments. In B, data acquired
380 on day 10 was compared with a one-way ANOVA with Holm-Sidak's multiple comparison test.
381 In E, data from each day was compared with a two-way ANOVA. Bars represent the mean \pm
382 SEM * denotes $p < 0.05$, ** denotes $p < 0.005$, **** denotes $p < 0.00005$.

383

384 **Figure 3: Trogocytosis strip Her2 from SKOV3 target cells**

385 (A) Her2 CAR GFP or control GFP macrophages were incubated with SKOV3 cells (mCh-
386 CAAX) for 2 hours. The cells were then stained for Her2 and analyzed by flow cytometry. A
387 representative flow plot shows the Her2 levels on SKOV3 cells alone (pink), and SKOV3 cells
388 incubated with Her2 CAR (blue) or control GFP macrophages (green). SKOV3 cells were also
389 stained with an isotype control antibody as a negative control (grey). (B) Graph shows the
390 median fluorescence intensity from three independent replicates. Bars represent the mean \pm

391 SEM of the replicates. Data was compared using a one way ANOVA with a Holm-Sidak multiple
392 comparison test. Data collected on the same day is annotated with the same shape point. *
393 denotes $p < 0.05$.

394

395 **Figure 4: Trogocytosis is more common than phagocytosis in multiple adherent cancer**
396 **cell lines**

397 Cancer cells were opsonized with a mouse anti-human CD47 antibody, and the amount of
398 phagocytosis and trogocytosis was measured by flow cytometry. (A) Representative flow plots
399 show the assay for distinguishing phagocytosis and trogocytosis by flow cytometry. (B) Graph
400 shows the percent of mCherry positive macrophages, indicating that these macrophages
401 internalized some cancer cell material. (C) Graph shows the fraction of mCherry positive
402 macrophages that were also positive for iRFP, indicating cancer cell phagocytosis (grey), or
403 lacking iRFP, indicating trogocytosis (pink). For B and C, data was compared using one-way
404 ANOVA with Holm-Sidak multiple comparison correction. N = 4 independent experiments,
405 consisting of 3 averaged technical replicates. Bars represent the mean \pm SEM. Data collected
406 on the same day is annotated with the same shape point. * denotes $p < 0.05$, ** denotes $p < 0.005$.
407

408 **Figure 5: Reducing cancer cell adhesion promotes phagocytosis**

409 (A) Her2 CAR GFP or control GFP-CAAX macrophages were incubated with adherent SKOV3
410 cells, RGD peptide treated SKOV3 cells, or suspended SKOV3 cells for 8 hours. The percent of
411 macrophages that phagocytosed (right) and trogocytosed (left) was measured during an 8 hour
412 timelapse. (B) SKOV3 cells with a membrane tethered mCherry (mCh-CAAX) and a nuclear
413 iRFP (H2B-iRFP) were plated with 50 $\mu\text{g}/\text{mL}$ RGD peptide 8 hours prior to macrophage addition
414 to block adhesion. (C) SKOV3 cells expressing mCherry-CAAX and H2B-iRFP were infected
415 with CRISPR-Cas9 and a sgRNA targeting integrin $\beta 1$, $\beta 5$, αV or a non targeting control guide
416 (NT). Infected cells were selected with puromycin and knockdown was confirmed by flow

417 cytometry (Fig. S4). The resulting polyclonal cell lines were incubated with Her2 CAR GFP or
418 control GFP-CAAX macrophages and the percent of macrophages that phagocytosed (left) and
419 trogocytosed (right) was measured during an 8 hour timelapse. Data was compared using one-
420 way ANOVA with Holm-Sidak multiple comparison correction. N = 4 independent experiments.
421 Bars represent the mean \pm SEM. Data collected on the same day is annotated with the same
422 shape point. * denotes $p < 0.05$, ** denotes $p < 0.005$, *** denotes $p < 0.0005$, **** denotes
423 $p < 0.00005$. Scale bars denote 20 μm .

424

425

426 **Figure 6: Increasing cancer cell adhesion reduces cancer cell phagocytosis**

427 (A) Raji B cells were infected with E cadherin GFP (CDH1 OE) to induce cell-cell adhesion.
428 Bright field images show the formation of cell clusters in CDH1 overexpressing cells. (B) Raji B
429 cells expressing H2B-iRFP were opsonized with a CD47 antibody and incubated with mCh-
430 CAAX macrophages for 2 hours. The percent of phagocytic macrophages was measured by
431 flow cytometry. Scale bars denote 500 μm . (C) Raji B cells expressing iRFP-CAAX were
432 opsonized with a CD47 antibody and incubated with mCh-CAAX macrophages for 2 hours. The
433 percent of iRFP positive macrophages was measured by flow cytometry. Data was compared
434 using one-way ANOVA with Holm-Sidak multiple comparison correction. N = 4 independent
435 experiments. Bars represent the mean \pm SEM. Data collected on the same day is annotated
436 with the same shape point. ** denotes $p < 0.005$.

437

438

439 **Figure 7: Mitotic cells are phagocytosed more than their interphase neighbors**

440 (A) Stills from Video 6 show a Her2 CAR GFP (green) macrophage phagocytosing a mitotic
441 SKOV3 (mCherry-CAAX, magenta). (B) Graph shows the fraction of SKOV3 undergoing division
442 in the entire population (left) compared to the fraction of phagocytosed SKOV3 cells undergoing

443 division (right). (C) SKOV3 cells expressing FUCCI were treated with 0.1 μ M paclitaxel or 1 μ M
444 STLC for 20 hours to arrest cells in mitosis. Image shows cells in G1 phase (blue; hCdt1) and
445 S/G2/M (magenta; hGeminin). (D) SKOV3 cells were treated with paclitaxel or STLC for 20
446 hours, then the inhibitors were removed and replaced with fresh media and Her2 CAR GFP
447 macrophages. The fraction of mCherry+ FUCCI SKOV3 cells (indicating S/G2/M phase) was
448 measured for the entire SKOV3 population (Total) and for the SKOV3 cells that were
449 phagocytosed (Of Phagocytosed Cells) during a 4 hour timelapse. (E) Graph shows the percent
450 of Her2 CAR GFP or GFP-CAAX macrophages phagocytosing a cancer cell in the same
451 experiment. For B, data was compared using a Students T test. N= 3 independent experiments.
452 For D and E, data was compared using one-way ANOVA with Holm-Sidak multiple comparison
453 correction. N = 4 independent experiments. Bars represent the mean \pm SEM. Data collected on
454 the same day is annotated with the same shape point. * denotes $p < 0.05$, ** denotes $p < 0.005$,
455 **** denotes $p < 0.00005$. Scale bars denote 20 μ m.

456

457

458 **Video legends**

459

460 **Video 1: Her2 CAR macrophage phagocytoses a SKOV3 cell**

461 Video shows Her2 CAR GFP (green) macrophage phagocytosing a SKOV3 cell (mCh-CAAX).

462 Images were acquired on a spinning disc confocal every 4 minutes. Scale bar is 20 μm . Stills

463 from this movie are shown in Figure 1.

464

465 **Video 2: Her2 CAR macrophage trogocytoses a SKOV3 cell**

466 Video shows Her2 CAR GFP (green) macrophage trogocytosing a SKOV3 cell (mCh-CAAX).

467 Images were acquired on a spinning disc confocal every minute. Scale bar is 20 μm . Stills from

468 this movie are shown in Figure 1.

469

470 **Video 3: Her2 CAR macrophages infiltrate a SKOV3 spheroid**

471 Video moves through the Z planes of a SKOV3 (mCherry-CAAX; magenta) incubated with Her2

472 CAR GFP (green) macrophages. The magenta line highlights the boundary of the spheroid in

473 each slice. Scale bar denotes 40 μm . Images of a live, unfixed sample were acquired on a

474 spinning disc confocal 24 hours after the sample was encapsulated in matrigel with

475 macrophages. The distance between Z slices is 10 μm and the total depth is 120 μm .

476

477 **Video 4: GFP-CAAX macrophages infiltrate a SKOV3 spheroid**

478 Video moves through the Z planes of a SKOV3 (mCherry-CAAX; magenta) incubated with GFP-

479 CAAX (green) macrophages. The magenta line highlights the boundary of the spheroid in each

480 slice. Scale bar denotes 40 μm . Images of a live, unfixed sample were acquired on a spinning

481 disc confocal 24 hours after the sample was encapsulated in matrigel with macrophages. The

482 distance between Z slices is 10 μm and the total depth is 120 μm .

483

484 **Video 5: Her2 CAR macrophage phagocytoses a SKOV3 cell in 3D spheroid**

485 Video shows Her2 CAR GFP (green) macrophage phagocytosing a SKOV3 cell (mCh-CAAX) in
486 a 3D spheroid. Images were acquired on a spinning disc confocal every 6 minutes. Scale bar is
487 20 μm . Stills from this movie are shown in Figure S1.

488

489 **Video 6: Her2 CAR macrophage phagocytoses a dividing SKOV3 cell**

490 Video shows Her2 CAR GFP (green) macrophage phagocytosing a dividing SKOV3 cell (mCh-
491 CAAX). Images were acquired on a spinning disc confocal every minute. Scale bar is 20 μm .
492 Stills from this movie are shown in Figure 7.

493 **Methods**

494

495 **Experimental models**

496

497 **Cell lines**

498 SKOV3 and L929 cells were obtained from the ATCC. HL-60 cells were obtained from
499 the Denise Montell lab at the University of California, Santa Barbara. HCT116 cells were
500 obtained from the Chris Richardson lab at the University of California, Santa Barbara. PANC-1
501 cells were obtained from the Angela Pitennis lab at the University of California, Santa Barbara.
502 Lenti-X 293T cells were purchased from Takara. SKOV3 and HCT116 cells were cultured in
503 McCoy's 5A (Fisher 16-600-108), 10% FBS, 1% PSG. PANC-1, L929, and 293T cells were
504 cultured in DMEM (Fisher 11965118), 10% FBS, 1% PSG. HL-60 cells were cultured in IMDM
505 (Fisher 12440061). Raji cells were cultured in RPMI with 1% Glutimax (Fisher 72400120), 10%
506 FBS, 1% PSG. Cells were routinely tested for mycoplasma. Cells were used for <20 passages.

507

508 **Lentivirus production**

509 pMD2.G (Gift from Didier Trono, VSV-G plasmid, Addgene plasmid 12259), pCMV-
510 dR8.2 (Gift from Bob Weinberg, Addgene plasmid 8455) (Stewart et al., 2003), and our target
511 construct was cloned into the pHR backbone. Transgene plasmids were transfected with
512 lipofectamine LTX (Invitrogen 15338-100) into HEK293T cells to generate lentivirus. The media
513 was harvested at 72hr, drawn through a 0.45um filter, and concentrated in LentiX (Takara
514 Biosciences 631232).

515

516 **Bone marrow derived macrophage cell culture**

517 Male and Female C57BL/6 mice between the ages of 6 to 10 weeks were sacrificed by
518 CO2 inhalation. Hips, femurs, tibia, and shoulders were dissected and bone marrow was

519 isolated according to Weischenfelt and Porse (Weischenfeldt & Porse, 2008). Bone marrow
520 cells were differentiated in complete RPMI supplemented with 20% L929-conditioned media for
521 7 days in a humidified incubator with 5% CO₂ at 37C. Fresh BMDM media was applied every 2-
522 3 days. Macrophage progenitors were infected with the lentiviruses Her2 CAR, GFP-CAAX, or
523 mCh-CAAX on day 5 post-harvest. Differentiated BMDMs were used for experiments from 7-10
524 days. Macrophage differentiation was confirmed by CD11b and F4/80 staining with >80%
525 double positive.

526

527 **Spheroid production**

528 Low-adhesion dishes were prepared by coating the wells of a tissue culture treated 96
529 well plate (Fisher Scientific 087722C) with 1.5% agarose. SKOV3 cells were plated at 8,000
530 cells per well in normal growth medium supplemented with 2.5% of reconstituted basement
531 membrane (rBM), Matrigel (Corning CB-40230C). Plates were centrifuged at 1000 rpm for 10
532 min at 4C to aggregate a plane of cells for spheroid formation. Cells were incubated for 72
533 hours at 37C upon which compact spheroids could be observed.

534

535

536 **Methods details**

537

538 **Plasmids**

539 Her2 CAR GFP was constructed in the pHR vector as follows: Signal peptide-
540 (MQSGTHWRVLGLCLLSVGVWGQD) derived from CD3ε; Extracellular- anti-HER2 (4D5-8)
541 scFv (Carter et al., 1992); stalk and TM- aa 138–206 CD8 (Uniprot Q96QR6_HUMAN); R
542 (single arginine insertion from cloning process); cytoplasmic domain (aa 45–86) of the Fc γ-
543 chain UniProtKB - P20491 (FCERG_MOUSE); linker- GSGS; Fluorophore: mGFP.

544

545 H2B-iRFP contains H2B (Uniprot H2B1B_HUMAN) inserted into the pHR vector; Fluorophore
546 iRFP₇₁₀.

547

548 CDH1-eGFP contains CDH1 (AddGene 133805 (Toda et al., 2018)) inserted into the puromycin
549 resistant and doxycycline inducible pCW57 vector (AddGene 71782 (Barger et al., 2019));
550 Fluorophore eGFP.

551

552 The GFP-CAAX in the pHR vector (Morrissey et al., 2018) contains eGFP fused to a C-terminal
553 CAAX targeting motif: KMSKDGKKKKKSKTKCVIM

554

555 mCh-CAAX in the pHR vector (Morrissey et al., 2018) contains mCh fused to a C-terminal
556 CAAX targeting motif: KMSKDGKKKKKSKTKCVIM

557

558 The iRFP-CAAX in the pHR vector (AddGene 170464 (Harris et al., 2021)) contains an iRFP₆₇₀
559 fused to a C-terminal CAAX targeting motif: KMSKDGKKKKKSKTKCVIM

560

561 **Flow cytometry measurement of trogocytosis and phagocytosis**

562 For adherent solid tumor cell lines, 35,000 cells were plated in 1 well of a 12 well dish
563 and incubated overnight prior to the experiment. For suspended targets, including solid or
564 diffuse tumors, 75,000 cells were directly added to 1 well of a 12 well dish at the time of
565 experimentation. These plating conditions both resulted in ~75,000 cell targets at the time of the
566 experiment. For antibody opsonization, purified mouse anti-human CD47 (Biolegend 323102,
567 RRID:AB_756132) was spiked into the wells of cancer cells at a concentration of 5ug/mL. To
568 achieve a ~1:1 ratio of effector to target cell ratio, 75,000 Her2 CAR or GFP BMDMs were
569 added to each well. BMDMs and cancer cells were co-incubated for 2 hrs, harvested in 0.25%
570 trypsin EDTA (Fisher 25200072), neutralized, then washed in cold PBS. Samples were
571 analyzed in an Attune NxT (Invitrogen). Further analysis was conducted in FlowJo. BMDMs
572 were gated by GFP+ single cells, then internalization of cancer cells was distinguished for
573 trogocytosis by mCh+/iRFP- and phagocytosis by mCh+/iRFP+ events.

574

575 **Timelapse microscopy of macrophage activity in 2D monolayers**

576 Unless otherwise specified, SKOV3 and macrophage co-incubations were performed
577 with adherent SKOV3 and macrophages added in suspension. 10,000 SKOV3 were plated in 1
578 well of a 96 well glass bottom Matriplate (Brooks, MGB096-1-2-LG-L) and incubated overnight
579 to establish adhesion. SKOV3 count approximately doubled overnight, yielding 20,000 cells. To
580 achieve a ~1:1 effector to target cell ratio, 20,000 Her2 CAR or GFP BMDMs were added to
581 each well the following day. Co-incubations were imaged using spinning disc microscopy (40 ×
582 0.95 NA Plan Apo air) for 8-10 hours with time intervals of 6 min or less. Internalized cancer
583 cells were classified for trogocytosis or phagocytosis in ImageJ. Trogocytosis was classified as
584 BMDMs that ingested fragments of the target cell membrane. Phagocytosis was classified as
585 BMDMs that engulfed the target cell whole.

586 In figures 5A and S3, suspended SKOV3 cells were added to adherent macrophages at
587 the start of the timelapse experiment at a 1:1 ratio of 20,000 macrophages:20,000 targets.

588 Mitotic mCh-CAAX SKOV3 were classified by the retraction of membrane to a round
589 mother cell, formation of a cleavage furrow or the appearance of a daughter cell. Phagocytosis
590 of a mitotic target was verified by any of the indicated hallmarks of mitosis.

591

592 **Spheroid size measurements**

593 After 72 hours on low adhesion plates, the resulting SKOV3 spheroids were transferred
594 to a Matrigel dome of 50:50 rBM and NGM. BMDMs were added at 500,000 cells per dome to
595 the liquid Matrigel. Domes were incubated at 37C for 30min to set the matrix before 500uL of
596 NGM was added to the well. Whole spheroids were removed from the incubator and imaged
597 daily for 10 days via spinning disc microscopy (10 × 0.95 NA Plan Apo air). Large images were
598 captured in Nikon Elements by stitching together a grid of 4 images using the large image tool
599 (15% overlap). The diameter of mCherry signal (mCherry-CAAX from SKOV3 cells and
600 internalized mCherry in macrophages) was measured in both the X and Y dimension in ImageJ.
601 The X and Y diameter was averaged to obtain the final spheroid diameter.

602

603 **Quantification of trogocytosis and phagocytosis in spheroids**

604 Spheroid macrophage co-incubations were imaged via spinning disc microscopy (40x
605 1.15 NA WI). BMDM activity was characterized in ImageJ by using mCherry-CAAX, H2B-iRFP
606 SKOV3 cells to distinguish trogocytosis (mCherry+,iRFP-) and phagocytosis (mCherry+,
607 iRFP+). 100um Z-stacks were captured at 2um steps. Only BMDMs that made contact with the
608 spheroid were analyzed.

609

610 **Macrophage invasion in spheroids**

611 Using Imaris 10.1, 10x spheroid Z-stacks were cropped to fit the spheroid dimensions,
612 reducing excess background signal. The SKOV3 fluorescent membrane signal was thresholded

613 to generate a reconstructed spheroid surface. The reconstructed surface was overlaid to each
614 slice of the Z-stack for ease of visualizing macrophages that had invaded into the spheroid.

615

616 **Her2 expression measurement**

617 35,000 mCh-CAAX H2B-iRFP SKOV3 were plated in 1 well of a 12 well dish and
618 incubated overnight prior to the experiment. 75,000 Her2 CAR or GFP BMDMs were added to
619 each well except single cell controls. BMDMs and cancer cells were co-incubated for 2 hrs,
620 harvested in 0.25% trypsin EDTA, neutralized, then blocked in incubation buffer (PBS + 0.5%
621 BSA) for 10 min. Cells were resuspended in incubation buffer for 30 min with either Brilliant
622 Violet 421 isotype control (BioLegend 400157; RRID:AB_10897939) or Anti-CD340 BV421
623 (BioLegend 324420; RRID:AB_2563990). Samples were triple washed in PBS then analyzed in
624 an Attune NxT. Further analysis was conducted in FlowJo to isolate the cancer cells and assess
625 the median fluorescence intensity of each sample.

626

627 **RGD peptide treatment**

628 For RGD peptide treated cells, 20,000 SKOV3 cells were seeded in media
629 supplemented with 50ug/mL of cilengitide trifluoroacetate salt (VWR International 88968-51-6).
630 Media was aspirated and replaced with fresh media immediately before adding 20,000
631 macrophages. Trogocytosis and phagocytosis were measured by timelapse microscopy as
632 described above.

633

634 **Focal adhesion CRISPR knockout generation and validation**

635 Focal adhesion knockouts were generated by digesting the guide scaffold of
636 LentiCRISPR v2 (Addgene plasmid 52961) and replacing it with the top guides of ITGB1,
637 ITGB5, ITGAV, and a non-targeting guide from the GeCKO v2 library (Table S1 (Sanjana et al.,

638 2014). mCh-CAAX H2B-iRFP SKOV3 were infected with the lentivirus, and infected cells were
639 selected with puromycin.

640 Integrin knockouts were validated for absence of surface expression via antibody
641 staining. The SKOV3 integrin knockout cell lines were harvested in 0.25% trypsin EDTA,
642 neutralized, washed in cold PBS, then blocked in incubation buffer for 10 min. Cells were
643 resuspended in incubation buffer for 30 min with the following antibodies: FITC ITGB5 IgG1
644 kappa (Thermo 11-0497-41, RRID:AB_2043843), FITC isotype control IgG1 kappa (Thermo 11-
645 4714-81, RRID:AB_470021), FITC ITAV/CD51 IgG2a kappa (BioLegend 327907,
646 RRID:AB_940558), or FITC isotype control IgG2a kappa (BioLegend 400210,
647 RRID:AB_326458). Samples were triple washed in PBS then analyzed in an Attune NxT.
648 Analysis was conducted in FlowJo to assess the median fluorescence intensity of each sample.

649

650 **E-cadherin overexpression**

651 iRFP₆₇₀-CAAX or H2B-iRFP₇₁₀ Raji were infected with CDH1-eGFP and underwent
652 puromycin selection to select for infected cells. 20,000 cells were plated into 1 well of a 12 well.
653 To achieve the E-cadherin overexpression, cells were treated with doxycycline for 72 hr prior to
654 the experiment. At the time of the experiment, control iRFP₆₇₀-CAAX or H2B-iRFP₇₁₀ Raji were
655 added at 450,000 cells to 1 well of a 12 well, adjusted to the count of the E-cadherin
656 overexpression cells. Cells were treated with purified mouse anti-human CD47 (Biolegend
657 323102, RRID:AB_756132) at a concentration of 5ug/mL. 450,000 BMDMs were seeded into
658 each well and co-incubated for 2hrs. BMDMs and cancer cells were co-incubated for 2 hrs,
659 harvested in 0.25% trypsin EDTA, neutralized, then washed in cold PBS. Samples were
660 analyzed in an Attune NxT. Further analysis was conducted in FlowJo. BMDMs were gated by
661 area/aspect ratio, mCh+ events. Within the mCh+ BMDM gate, phagocytosis was determined by
662 the iRFP+ events from H2B-iRFP₇₁₀ samples, whereas total activity was determined by the
663 iRFP+ events from iRFP₆₇₀-CAAX.

664

665 **Cell cycle arrest**

666 Cells were treated with 0.1 μ M paclitaxel (ThermoFisher P3456) or 1 μ M STLC (Sigma
667 164739-5G) for 20 hr prior to the experiment. To quantify cell cycle arrest, SKOV3 cells were
668 infected with the FUCCI cell cycle reporter mCherry(G1)/BFP(S/G2) (Addgene plasmid
669 132429)(Sato et al., 2019). mCherry+ cells were considered to be in G1 and BFP+ cells were
670 counted as S/G2/M. Timelapse imaging was used to measure phagocytosis as described
671 above.

672

673 **Phosphatidylserine staining**

674 To measure phosphatidylserine, cells were stained with Pacific Blue Annexin
675 (BioLegend 640918, RRID:AB_1279046). 35,000 SKOV3 cells were plated into 1 well of a 12
676 well and incubated overnight before treatment with a mitotic inhibitor for 20 hours. SKOV3
677 treated with 250 μ M Hydrogen peroxide for 20 hours served as a positive control for death. Cells
678 were harvested in 0.25% trypsin EDTA, neutralized, washed in cold PBS, then blocked in
679 incubation buffer for 10 min. Cells were resuspended in annexin binding buffer for 30 min with
680 Pacific Blue Annexin. Samples were triple washed in PBS then analyzed in an Attune NxT.

681

682 **Microscopy**

683 Fluorescent images were acquired on a spinning disc confocal microscope (Nikon Ti2-E
684 inverted microscope with a Yokogawa CSU-W1 spinning disk unit and a Hamamatsu Orca
685 Fusion BT scMos camera). Objectives included 10 x 0.45 NA Plan Apo air, 40 x 0.95 NA Plan
686 Apo air, 40 x 1.15 NA water immersion, and a 100 x 1.49 NA oil immersion. The microscope is
687 equipped with a piezo Z drive. Temperature, CO₂, and humidity were controlled via an OkoLabs
688 stage top incubator. Image acquisition was controlled using Nikon Elements.

689 Brightfield images were acquired on an inverted ECHO Revolve with the 10 x 0.35 NA

690 Plan Apo air objective. Image acquisition was controlled using ECHO software.

691

692 **Statistical analysis**

693 All statistical analyses were performed in Prism 10 (GraphPad) and presented as mean

694 values and standard error of the mean. Figure legends indicate the statistical test performed

695 and the number of biological replicates. In flow cytometry experiments, three technical replicates

696 were averaged to calculate the biological replicate.

697

698

699 **Acknowledgements**

700

701 We thank the members of the Morrissey Lab for their constructive feedback and advice.

702 We also thank Ryan Stowers for advice on the 3D culture system. This work was supported by

703 NIGMS R35 GM146935 and University of California Cancer Research Coordinating Committee

704 seed grant C23CR5592. M.M. is a Nadia's Gift Foundation Innovator of the Damon Runyon

705 Cancer Research Foundation (DRR-85-25). K.R. was supported by the UCSB Graduate

706 Division Graduate Research Mentorship Program Fellowship and UCSB Graduate Division

707 Research Accelerator Award. We acknowledge the use of the NRI-MCDB Microscopy Facility

708 (Imaris) supported by the NIH: 1S10 ODO010610-01A1. Illustrations were prepared in

709 BioRender.

710

711

712

713 **References**

714

715 Abdu, Y., Maniscalco, C., Heddleston, J. M., Chew, T.-L., & Nance, J. (2016). Developmentally
716 programmed germ cell remodelling by endodermal cell cannibalism. *Nature Cell Biology*,
717 *18*(12), 1302–1310. <https://doi.org/10.1038/ncb3439>

718 Akhmanova, M., Emtenani, S., Krueger, D., Gyoergy, A., Guarda, M., Vlasov, M., Vlasov, F.,
719 Akopian, A., Ratheesh, A., De Renzis, S., & Siekhaus, D. E. (2022). Cell division in
720 tissues enables macrophage infiltration. *Science*, *376*(6591), 394–396.
721 <https://doi.org/10.1126/science.abj0425>

722 Arandjelovic, S., & Ravichandran, K. S. (2015). Phagocytosis of apoptotic cells in homeostasis.
723 *Nature Immunology*, *16*(9), 907–917. <https://doi.org/10.1038/ni.3253>

724 Barger, C. J., Branick, C., Chee, L., & Karpf, A. R. (2019). Pan-Cancer Analyses Reveal
725 Genomic Features of FOXM1 Overexpression in Cancer. *Cancers*, *11*(2), 251.
726 <https://doi.org/10.3390/cancers11020251>

727 Bettadapur, A., Miller, H. W., & Ralston, K. S. (2020). Biting off what can be chewed:
728 Trophocytosis in health, infection, and disease. *Infection and Immunity*, *88*(7).
729 <https://doi.org/10.1128/IAI.00930-19>

730 Beum, P. V., Peek, E. M., Lindorfer, M. A., Beurskens, F. J., Engelberts, P. J., Parren, P. W. H.
731 I., van de Winkel, J. G. J., & Taylor, R. P. (2011). Loss of CD20 and bound CD20
732 antibody from opsonized B cells occurs more rapidly because of trophocytosis mediated
733 by Fc receptor-expressing effector cells than direct internalization by the B cells. *Journal*
734 *of Immunology (Baltimore, Md. : 1950)*, *187*(6), 3438–3447.
735 <https://doi.org/10.4049/JIMMUNOL.1101189>

736 Brancolini, C., Lazarevic, D., Rodriguez, J., & Schneider, C. (1997). Dismantling Cell–Cell
737 Contacts during Apoptosis Is Coupled to a Caspase-dependent Proteolytic Cleavage of
738 β -Catenin. *Journal of Cell Biology*, *139*(3), 759–771.

- 739 <https://doi.org/10.1083/jcb.139.3.759>
- 740 Carter, P., Presta, L., Gorman, C. M., Ridgway, J. B., Henner, D., Wong, W. L., Rowland, A. M.,
741 Kotts, C., Carver, M. E., & Shepard, H. M. (1992). Humanization of an anti-p185HER2
742 antibody for human cancer therapy. *Proceedings of the National Academy of Sciences*,
743 89(10), 4285–4289. <https://doi.org/10.1073/pnas.89.10.4285>
- 744 Casey, R. C., Burleson, K. M., Skubitz, K. M., Pambuccian, S. E., Oegema, T. R., Ruff, L. E., &
745 Skubitz, A. P. N. (2001). B1-Integrins Regulate the Formation and Adhesion of Ovarian
746 Carcinoma Multicellular Spheroids. *The American Journal of Pathology*, 159(6), 2071–
747 2080.
- 748 Chao, M. P., Alizadeh, A. A., Tang, C., Myklebust, J. H., Varghese, B., Gill, S., Jan, M., Cha, A.
749 C., Chan, C. K., Tan, B. T., Park, C. Y., Zhao, F., Kohrt, H. E., Malumbres, R., Briones,
750 J., Gascoyne, R. D., Lossos, I. S., Levy, R., Weissman, I. L., & Majeti, R. (2010). Anti-
751 CD47 Antibody Synergizes with Rituximab to Promote Phagocytosis and Eradicate Non-
752 Hodgkin Lymphoma. *Cell*, 142(5), 699–713. <https://doi.org/10.1016/j.cell.2010.07.044>
- 753 Chen, X., Song, X., Li, K., & Zhang, T. (2019). FcγR-Binding Is an Important Functional Attribute
754 for Immune Checkpoint Antibodies in Cancer Immunotherapy. *Frontiers in Immunology*,
755 10, 292. <https://doi.org/10.3389/fimmu.2019.00292>
- 756 Cornell, C. E., Chorlay, A., Krishnamurthy, D., Martin, N. R., Baldauf, L., & Fletcher, D. A.
757 (2024). *Target cell tension regulates macrophage trogocytosis* (p. 2024.12.02.626490).
758 bioRxiv. <https://doi.org/10.1101/2024.12.02.626490>
- 759 Cruet-Hennequart, S., Maubant, S., Luis, J., Gauduchon, P., Staedel, C., & Dedhar, S. (2003).
760 Av integrins regulate cell proliferation through integrin-linked kinase (ILK) in ovarian
761 cancer cells. *Oncogene*, 22(11), 1688–1702. <https://doi.org/10.1038/sj.onc.1206347>
- 762 Dahan, R., Barnhart, B. C., Li, F., Yamniuk, A. P., Korman, A. J., & Ravetch, J. V. (2016).
763 Therapeutic Activity of Agonistic, Human Anti-CD40 Monoclonal Antibodies Requires
764 Selective FcγR Engagement. *Cancer Cell*, 29(6), 820–831.

- 765 <https://doi.org/10.1016/j.ccell.2016.05.001>
- 766 Davidson, B., Goldberg, I., Reich, R., Tell, L., Dong, H. P., Trope', C. G., Risberg, B., &
767 Kopolovic, J. (2003). AlphaV- and beta1-integrin subunits are commonly expressed in
768 malignant effusions from ovarian carcinoma patients. *Gynecologic Oncology*, *90*(2),
769 248–257. [https://doi.org/10.1016/s0090-8258\(03\)00321-4](https://doi.org/10.1016/s0090-8258(03)00321-4)
- 770 de Visser, K. E., & Joyce, J. A. (2023). The evolving tumor microenvironment: From cancer
771 initiation to metastatic outgrowth. *Cancer Cell*, *41*(3), 374–403.
772 <https://doi.org/10.1016/j.ccell.2023.02.016>
- 773 Dechantsreiter, M. A., Planker, E., Mathä, B., Lohof, E., Hölzemann, G., Jonczyk, A., Goodman,
774 S. L., & Kessler, H. (1999). N-Methylated Cyclic RGD Peptides as Highly Active and
775 Selective $\alpha V\beta 3$ Integrin Antagonists. *Journal of Medicinal Chemistry*, *42*(16), 3033–
776 3040. <https://doi.org/10.1021/jm970832g>
- 777 Desgrosellier, J. S., & Cheresh, D. A. (2010). Integrins in cancer: Biological implications and
778 therapeutic opportunities. *Nature Reviews. Cancer*, *10*(1), 9–22.
779 <https://doi.org/10.1038/nrc2748>
- 780 Dix, C. L., Matthews, H. K., Uroz, M., McLaren, S., Wolf, L., Heatley, N., Win, Z., Almada, P.,
781 Henriques, R., Boutros, M., Trepä, X., & Baum, B. (2018). The Role of Mitotic Cell-
782 Substrate Adhesion Re-modeling in Animal Cell Division. *Developmental Cell*, *45*(1),
783 132-145.e3. <https://doi.org/10.1016/j.devcel.2018.03.009>
- 784 Dooling, L. J., Andrechak, J. C., Hayes, B. H., Kadu, S., Zhang, W., Pan, R., Vashisth, M.,
785 Irianto, J., Alvey, C. M., Ma, L., & Discher, D. E. (2023). Cooperative phagocytosis of
786 solid tumours by macrophages triggers durable anti-tumour responses. *Nature*
787 *Biomedical Engineering*, *7*(9), 1081–1096. <https://doi.org/10.1038/s41551-023-01031-3>
- 788 Dooling, L. J., Anlaş, A. A., Tobin, M. P., Ontko, N. M., Marchena, T., Wang, M., Andrechak, J.
789 C., & Discher, D. E. (2024). *Clustered macrophages cooperate to eliminate tumors via*
790 *coordinated intrudopodia* (p. 2024.09.19.613918). bioRxiv.

- 791 <https://doi.org/10.1101/2024.09.19.613918>
- 792 Fesnak, A. D., June, C. H., & Levine, B. L. (2016). Engineered T cells: The promise and
793 challenges of cancer immunotherapy. *Nature Reviews Cancer*, *16*(9), 566–581.
794 <https://doi.org/10.1038/nrc.2016.97>
- 795 Finotti, G., Pietronigro, E., Balanzin, C., Lonardi, S., Constantin, G., Chao, M. P., Tecchio, C.,
796 Vermi, W., & Cassatella, M. A. (2023). Slan+ Monocytes Kill Cancer Cells Coated in
797 Therapeutic Antibody by Trogoptosis. *Cancer Immunology Research*, *11*(11), 1538–
798 1552. <https://doi.org/10.1158/2326-6066.CIR-23-0239>
- 799 Freeman, S., & Grinstein, S. (2021). Promoters and Antagonists of Phagocytosis: A Plastic and
800 Tunable Response. *Annual Review of Cell and Developmental Biology*, *37*, 89–114.
801 <https://doi.org/10.1146/annurev-cellbio-120219-055903>
- 802 Gao, X., Carpenter, R. S., Boulais, P. E., Zhang, D., Marlein, C. R., Li, H., Smith, M., Chung, D.
803 J., Maryanovich, M., Will, B., Steidl, U., & Frenette, P. S. (2024). Regulation of the
804 hematopoietic stem cell pool by C-Kit–associated trogocytosis. *Science*, *385*(6709),
805 eadp2065. <https://doi.org/10.1126/science.adp2065>
- 806 Giordano, S. H., Franzoi, M. A. B., Temin, S., Anders, C. K., Chandarlapaty, S., Crews, J. R.,
807 Kirshner, J. J., Krop, I. E., Lin, N. U., Morikawa, A., Patt, D. A., Perlmutter, J.,
808 Ramakrishna, N., & Davidson, N. E. (2022). Systemic Therapy for Advanced Human
809 Epidermal Growth Factor Receptor 2–Positive Breast Cancer: ASCO Guideline Update.
810 *Journal of Clinical Oncology*, *40*(23), 2612–2635. <https://doi.org/10.1200/JCO.22.00519>
- 811 Gordon, S. (2016). Phagocytosis: An Immunobiologic Process. *Immunity*, *44*(3), 463–475.
812 <https://doi.org/10.1016/j.immuni.2016.02.026>
- 813 Guerriero, J. L. (2018). Macrophages: The Road Less Traveled, Changing Anticancer Therapy.
814 *Trends in Molecular Medicine*, *24*(5), 472–489.
815 <https://doi.org/10.1016/j.molmed.2018.03.006>
- 816 Gül, N., Babes, L., Siegmund, K., Korthouwer, R., Bögels, M., Braster, R., Vidarsson, G., ten

- 817 Hagen, T. L. M., Kubes, P., & van Egmond, M. (2014). Macrophages eliminate
818 circulating tumor cells after monoclonal antibody therapy. *The Journal of Clinical*
819 *Investigation*, 124(2), 812–823. <https://doi.org/10.1172/JCI66776>
- 820 Hamieh, M., Dobrin, A., Cabriolu, A., van der Stegen, S. J. C., Giavridis, T., Mansilla-Soto, J.,
821 Eyquem, J., Zhao, Z., Whitlock, B. M., Miele, M. M., Li, Z., Cunanan, K. M., Huse, M.,
822 Hendrickson, R. C., Wang, X., Rivière, I., & Sadelain, M. (2019). CAR T cell trogocytosis
823 and cooperative killing regulate tumour antigen escape. *Nature*, 568(7750), 112–116.
824 <https://doi.org/10.1038/s41586-019-1054-1>
- 825 Harris, M. J., Fuyal, M., & James, J. R. (2021). Quantifying persistence in the T-cell signaling
826 network using an optically controllable antigen receptor. *Molecular Systems Biology*,
827 17(5), e10091. <https://doi.org/10.15252/msb.202010091>
- 828 Heredia-Soto, V., Redondo, A., Berjón, A., Miguel-Martín, M., Díaz, E., Crespo, R., Hernández,
829 A., Yébenes, L., Gallego, A., Feliu, J., Hardisson, D., & Mendiola, M. (2018). High-
830 throughput 3-dimensional culture of epithelial ovarian cancer cells as preclinical model of
831 disease. *Oncotarget*, 9(31), 21893–21903. <https://doi.org/10.18632/oncotarget.25098>
- 832 Horwitz, S. B. (1994). Taxol (paclitaxel): Mechanisms of action. *Annals of Oncology: Official*
833 *Journal of the European Society for Medical Oncology*, 5 Suppl 6, S3-6.
- 834 Hudrisier, D., Riond, J., Mazarguil, H., Gairin, J. E., & Joly, E. (2001). Cutting edge: CTLs
835 rapidly capture membrane fragments from target cells in a TCR signaling-dependent
836 manner. *Journal of Immunology (Baltimore, Md. : 1950)*, 166(6), 3645–3649.
- 837 Hudziak, R. M., Lewis, G. D., Winget, M., Fendly, B. M., Shepard, H. M., & Ullrich, A. (1989).
838 p185HER2 monoclonal antibody has antiproliferative effects in vitro and sensitizes
839 human breast tumor cells to tumor necrosis factor. *Molecular and Cellular Biology*, 9(3),
840 1165–1172.
- 841 Ivascu, A., & Kubbies, M. (2007). Diversity of cell-mediated adhesions in breast cancer
842 spheroids. *International Journal of Oncology*, 31(6), 1403–1413.

- 843 Jaiswal, S., Jamieson, C. H. M., Pang, W. W., Park, C. Y., Chao, M. P., Majeti, R., Traver, D.,
844 van Rooijen, N., & Weissman, I. L. (2009). CD47 Is Upregulated on Circulating
845 Hematopoietic Stem Cells and Leukemia Cells to Avoid Phagocytosis. *Cell*, *138*(2), 271–
846 285. <https://doi.org/10.1016/j.cell.2009.05.046>
- 847 Joffe, A. M., Bakalar, M. H., & Fletcher, D. A. (2020). Macrophage phagocytosis assay with
848 reconstituted target particles. *Nature Protocols*, *15*(7), 2230–2246.
849 <https://doi.org/10.1038/s41596-020-0330-8>
- 850 Joly, E., & Hudrisier, D. (2003). What is trogocytosis and what is its purpose? *Nature*
851 *Immunology*, *4*(9), 815–815. <https://doi.org/10.1038/ni0903-815>
- 852 Kennedy, A. D., Beum, P. V., Solga, M. D., DiLillo, D. J., Lindorfer, M. A., Hess, C. E.,
853 Densmore, J. J., Williams, M. E., & Taylor, R. P. (2004). Rituximab Infusion Promotes
854 Rapid Complement Depletion and Acute CD20 Loss in Chronic Lymphocytic Leukemia1.
855 *The Journal of Immunology*, *172*(5), 3280–3288.
856 <https://doi.org/10.4049/jimmunol.172.5.3280>
- 857 Kern, N., Dong, R., Douglas, S. M., Vale, R. D., & Morrissey, M. A. (2021). Tight nanoscale
858 clustering of Fcγ receptors using DNA origami promotes phagocytosis. *eLife*, *10*,
859 e68311. <https://doi.org/10.7554/eLife.68311>
- 860 Klichinsky, M., Ruella, M., Shestova, O., Lu, X. M., Best, A., Zeeman, M., Schmierer, M.,
861 Gabrusiewicz, K., Anderson, N. R., Petty, N. E., Cummins, K. D., Shen, F., Shan, X.,
862 Veliz, K., Blouch, K., Yashiro-Ohtani, Y., Kenderian, S. S., Kim, M. Y., O'Connor, R. S.,
863 ... Gill, S. (2020). Human chimeric antigen receptor macrophages for cancer
864 immunotherapy. *Nature Biotechnology*, *38*(8), 947–953. <https://doi.org/10.1038/s41587-020-0462-y>
- 865
866 Kochenderfer, J. N., Feldman, S. A., Zhao, Y., Xu, H., Black, M. A., Morgan, R. A., Wilson, W.
867 H., & Rosenberg, S. A. (2009). Construction and Preclinical Evaluation of an Anti-CD19
868 Chimeric Antigen Receptor. *Journal of Immunotherapy*, *32*(7), 689–702.

- 869 <https://doi.org/10.1097/CJI.0b013e3181ac6138>
- 870 Lindorfer, M. A., & Taylor, R. P. (2022). FcγR-Mediated Trogocytosis 2.0: Revisiting History
871 Gives Rise to a Unifying Hypothesis. *Antibodies*, 11(3), 45.
872 <https://doi.org/10.3390/antib11030045>
- 873 Lock, J. G., Jones, M. C., Askari, J. A., Gong, X., Oddone, A., Olofsson, H., Göransson, S.,
874 Lakadamyali, M., Humphries, M. J., & Strömblad, S. (2018). Reticular adhesions are a
875 distinct class of cell-matrix adhesions that mediate attachment during mitosis. *Nature*
876 *Cell Biology*, 20(11), 1290–1302. <https://doi.org/10.1038/s41556-018-0220-2>
- 877 Majeti, R., Chao, M. P., Alizadeh, A. A., Pang, W. W., Jaiswal, S., Gibbs, K. D., van Rooijen, N.,
878 & Weissman, I. L. (2009). CD47 Is an Adverse Prognostic Factor and Therapeutic
879 Antibody Target on Human Acute Myeloid Leukemia Stem Cells. *Cell*, 138(2), 286–299.
880 <https://doi.org/10.1016/j.cell.2009.05.045>
- 881 Manches, O., Lui, G., Chaperot, L., Gressin, R., Molens, J.-P., Jacob, M.-C., Sotto, J.-J.,
882 Leroux, D., Bensa, J.-C., & Plumas, J. (2003). In vitro mechanisms of action of rituximab
883 on primary non-Hodgkin lymphomas. *Blood*, 101(3), 949–954.
884 <https://doi.org/10.1182/blood-2002-02-0469>
- 885 Marchesi, S., Montani, F., Deflorian, G., D'Antuono, R., Cuomo, A., Bologna, S., Mazzoccoli, C.,
886 Bonaldi, T., Di Fiore, P. P., & Nicassio, F. (2014). DEPDC1B Coordinates De-adhesion
887 Events and Cell-Cycle Progression at Mitosis. *Developmental Cell*, 31(4), 420–433.
888 <https://doi.org/10.1016/j.devcel.2014.09.009>
- 889 Matlung, H. L., Babes, L., Zhao, X. W., van Houdt, M., Treffers, L. W., van Rees, D. J., Franke,
890 K., Schornagel, K., Verkuijlen, P., Janssen, H., Halonen, P., Lieftink, C., Beijersbergen,
891 R. L., Leusen, J. H. W., Boelens, J. J., Kuhnle, I., van der Werff Ten Bosch, J., Seeger,
892 K., Rutella, S., ... van den Berg, T. K. (2018). Neutrophils Kill Antibody-Opsonized
893 Cancer Cells by Trogoptosis. *Cell Reports*, 23(13), 3946-3959.e6.
894 <https://doi.org/10.1016/J.CELREP.2018.05.082>

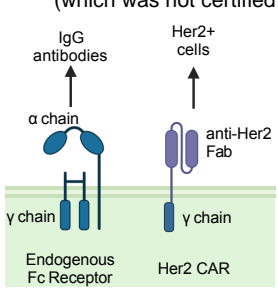
- 895 Mercer, F., Ng, S. H., Brown, T. M., Boatman, G., & Johnson, P. J. (2018). Neutrophils kill the
896 parasite *Trichomonas vaginalis* using trogocytosis. *PLoS Biology*, *16*(2).
897 <https://doi.org/10.1371/JOURNAL.PBIO.2003885>
- 898 Mishra, A. K., Rodriguez, M., Torres, A. Y., Smith, M., Rodriguez, A., Bond, A., Morrissey, M. A.,
899 & Montell, D. J. (2023). Hyperactive Rac stimulates cannibalism of living target cells and
900 enhances CAR-M-mediated cancer cell killing. *Proceedings of the National Academy of*
901 *Sciences of the United States of America*, *120*(52), e2310221120.
902 <https://doi.org/10.1073/pnas.2310221120>
- 903 Möller, J., Lühmann, T., Chabria, M., Hall, H., & Vogel, V. (2013). Macrophages lift off surface-
904 bound bacteria using a filopodium-lamellipodium hook-and-shovel mechanism. *Scientific*
905 *Reports*, *3*(1), 2884. <https://doi.org/10.1038/srep02884>
- 906 Morrissey, M. A., Williamson, A. P., Steinbach, A. M., Roberts, E. W., Kern, N., Headley, M. B.,
907 & Vale, R. D. (2018). Chimeric antigen receptors that trigger phagocytosis. *eLife*, *7*,
908 e36688. <https://doi.org/10.7554/eLife.36688>
- 909 Nimmerjahn, F., & Ravetch, J. V. (2008). Fcγ receptors as regulators of immune responses.
910 *Nature Reviews Immunology*, *8*(1), 34–47. <https://doi.org/10.1038/nri2206>
- 911 Osorio, J. C., Smith, P., Knorr, D. A., & Ravetch, J. V. (2023). The antitumor activities of anti-
912 CD47 antibodies require Fc-FcγR interactions. *Cancer Cell*, *41*(12), 2051-2065.e6.
913 <https://doi.org/10.1016/j.ccell.2023.10.007>
- 914 Park, H.-R., Kim, S.-E., Keam, B., Chung, H., Seok, S. H., Kim, S., Kim, M., Kim, T. M., Doh, J.,
915 Kim, D.-W., & Heo, D. S. (2022). Blockade of CD47 enhances the antitumor effect of
916 macrophages in renal cell carcinoma through trogocytosis. *Scientific Reports*, *12*(1),
917 12546. <https://doi.org/10.1038/s41598-022-16766-3>
- 918 Petricevic, B., Laengle, J., Singer, J., Sachet, M., Fazekas, J., Steger, G., Bartsch, R., Jensen-
919 Jarolim, E., & Bergmann, M. (2013). Trastuzumab mediates antibody-dependent cell-
920 mediated cytotoxicity and phagocytosis to the same extent in both adjuvant and

- 921 metastatic HER2/neu breast cancer patients. *Journal of Translational Medicine*, 11, 307.
922 <https://doi.org/10.1186/1479-5876-11-307>
- 923 Ralston, K. S., Solga, M. D., Mackey-Lawrence, N. M., Bhattacharya, A., & Petri Jr, W. A.
924 (2014). Trophocytosis by *Entamoeba histolytica* contributes to cell killing and tissue
925 invasion. *Nature*, 508. <https://doi.org/10.1038/nature13242>
- 926 Sakaue-Sawano, A., Kurokawa, H., Morimura, T., Hanyu, A., Hama, H., Osawa, H., Kashiwagi,
927 S., Fukami, K., Miyata, T., Miyoshi, H., Imamura, T., Ogawa, M., Masai, H., & Miyawaki,
928 A. (2008). Visualizing Spatiotemporal Dynamics of Multicellular Cell-Cycle Progression.
929 *Cell*, 132(3), 487–498. <https://doi.org/10.1016/j.cell.2007.12.033>
- 930 Sanjana, N. E., Shalem, O., & Zhang, F. (2014). Improved vectors and genome-wide libraries
931 for CRISPR screening. *Nature Methods*, 11(8), 783–784.
932 <https://doi.org/10.1038/nmeth.3047>
- 933 Sato, H., Wu, B., Delahaye, F., Singer, R. H., & Grealley, J. M. (2019). Retargeting of macroH2A
934 following mitosis to cytogenetic-scale heterochromatic domains. *Journal of Cell Biology*,
935 218(6), 1810–1823. <https://doi.org/10.1083/jcb.201811109>
- 936 Shi, Y., Fan, X., Deng, H., Brezski, R. J., Ryczyn, M., Jordan, R. E., Strohl, W. R., Zou, Q.,
937 Zhang, N., & An, Z. (2015). Trastuzumab triggers phagocytic killing of high HER2 cancer
938 cells in vitro and in vivo by interaction with Fcγ receptors on macrophages. *Journal of*
939 *Immunology (Baltimore, Md.: 1950)*, 194(9), 4379–4386.
940 <https://doi.org/10.4049/jimmunol.1402891>
- 941 Skoufias, D. A., DeBonis, S., Saoudi, Y., Lebeau, L., Crevel, I., Cross, R., Wade, R. H.,
942 Hackney, D., & Kozielski, F. (2006). S-Trityl-L-cysteine Is a Reversible, Tight Binding
943 Inhibitor of the Human Kinesin Eg5 That Specifically Blocks Mitotic Progression *.
944 *Journal of Biological Chemistry*, 281(26), 17559–17569.
945 <https://doi.org/10.1074/jbc.M511735200>
- 946 Sloas, C., Gill, S., & Klichinsky, M. (2021). Engineered CAR-Macrophages as Adoptive

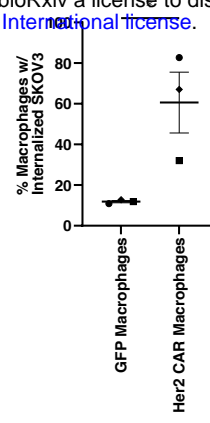
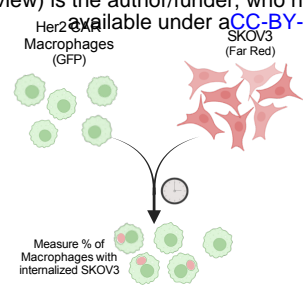
- 947 Immunotherapies for Solid Tumors. *Frontiers in Immunology*, 12, 783305.
948 <https://doi.org/10.3389/fimmu.2021.783305>
- 949 Stewart, S. A., Dykxhoorn, D. M., Palliser, D., Mizuno, H., Yu, E. Y., An, D. S., Sabatini, D. M.,
950 Chen, I. S. Y., Hahn, W. C., Sharp, P. A., Weinberg, R. A., & Novina, C. D. (2003).
951 Lentivirus-delivered stable gene silencing by RNAi in primary cells. *RNA (New York,*
952 *N. Y.)*, 9(4), 493–501. <https://doi.org/10.1261/rna.2192803>
- 953 Swain, S. M., Shastry, M., & Hamilton, E. (2023). Targeting HER2-positive breast cancer:
954 Advances and future directions. *Nature Reviews Drug Discovery*, 22(2), 101–126.
955 <https://doi.org/10.1038/s41573-022-00579-0>
- 956 Toda, S., Blauch, L. R., Tang, S. K. Y., Morsut, L., & Lim, W. A. (2018). Programming self-
957 organizing multicellular structures with synthetic cell-cell signaling. *Science (New York,*
958 *N. Y.)*, 361(6398), 156–162. <https://doi.org/10.1126/science.aat0271>
- 959 Tofani, L. B., Abriata, J. P., Luiz, M. T., Marchetti, J. M., & Swiech, K. (2020). Establishment and
960 characterization of an in vitro 3D ovarian cancer model for drug screening assays.
961 *Biotechnology Progress*, 36(6), e3034. <https://doi.org/10.1002/btpr.3034>
- 962 Uchida, J., Hamaguchi, Y., Oliver, J. A., Ravetch, J. V., Poe, J. C., Haas, K. M., & Tedder, T. F.
963 (2004). The innate mononuclear phagocyte network depletes B lymphocytes through Fc
964 receptor-dependent mechanisms during anti-CD20 antibody immunotherapy. *Journal of*
965 *Experimental Medicine*, 199(12), 1659–1669. <https://doi.org/10.1084/jem.20040119>
- 966 Van Wagoner, C. M., Rivera-Escalera, F., Jaimes-Delgadillo, N. C., Chu, C. C., Zent, C. S., &
967 Elliott, M. R. (2023). Antibody-mediated phagocytosis in cancer immunotherapy.
968 *Immunological Reviews*, 319(1), 128–141. <https://doi.org/10.1111/imr.13265>
- 969 Velmurugan, R., Challa, D. K., Ram, S., Ober, R. J., & Ward, E. S. (2016). Macrophage-
970 Mediated Trophocytosis Leads to Death of Antibody-Opsonized Tumor Cells. *Molecular*
971 *Cancer Therapeutics*, 15(8), 1879–1889. <https://doi.org/10.1158/1535-7163.MCT-15->
972 0335

973 Weinhard, L., Bartolomei, G. di, Bolasco, G., Machado, P., Schieber, N. L., Neniskyte, U.,
974 Exiga, M., Vadisiute, A., Raggioli, A., Schertel, A., Schwab, Y., & Gross, C. T. (2018).
975 Microglia remodel synapses by presynaptic trogocytosis and spine head filopodia
976 induction. *Nature Communications*, 9, 1228. <https://doi.org/10.1038/s41467-018-03566-5>
977 Weischenfeldt, J., & Porse, B. (2008). Bone Marrow-Derived Macrophages (BMM): Isolation and
978 Applications. *Cold Spring Harbor Protocols*, 2008(12), pdb.prot5080.
979 <https://doi.org/10.1101/pdb.prot5080>
980 Weiskopf, K., & Weissman, I. L. (2015). Macrophages are critical effectors of antibody therapies
981 for cancer. *mAbs*, 7(2), 303–310. <https://doi.org/10.1080/19420862.2015.1011450>
982 Williams, M. E., Densmore, J. J., Pawluczkwycz, A. W., Beum, P. V., Kennedy, A. D.,
983 Lindorfer, M. A., Hamil, S. H., Eggleton, J. C., & Taylor, R. P. (2006). Thrice-Weekly
984 Low-Dose Rituximab Decreases CD20 Loss via Shaving and Promotes Enhanced
985 Targeting in Chronic Lymphocytic Leukemia¹. *The Journal of Immunology*, 177(10),
986 7435–7443. <https://doi.org/10.4049/jimmunol.177.10.7435>
987 Zent, C. S., Taylor, R. P., Lindorfer, M. A., Beum, P. V., LaPlant, B., Wu, W., Call, T. G., Bowen,
988 D. A., Conte, M. J., Frederick, L. A., Link, B. K., Blackwell, S. E., Veeramani, S., Baig, N.
989 A., Viswanatha, D. S., Weiner, G. J., & Witzig, T. E. (2014). Chemoimmunotherapy for
990 relapsed/refractory and progressive 17p13-deleted chronic lymphocytic leukemia (CLL)
991 combining pentostatin, alemtuzumab, and low-dose rituximab is effective and tolerable
992 and limits loss of CD20 expression by circulating CLL cells. *American Journal of*
993 *Hematology*, 89(7), 757–765. <https://doi.org/10.1002/ajh.23737>

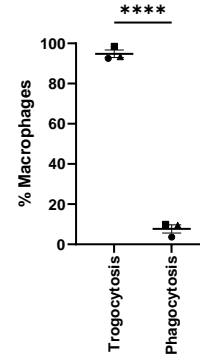
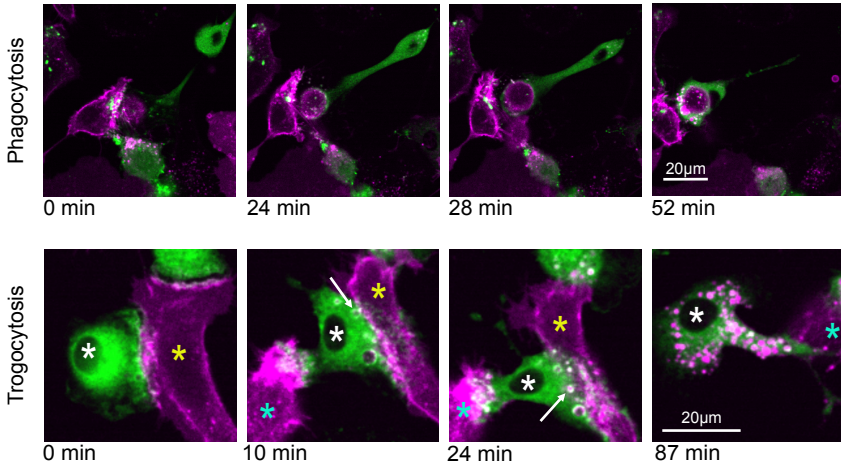
A

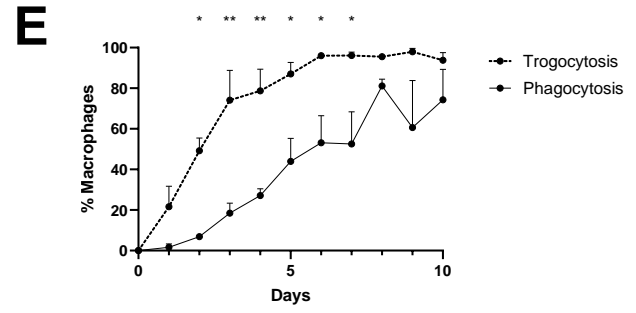
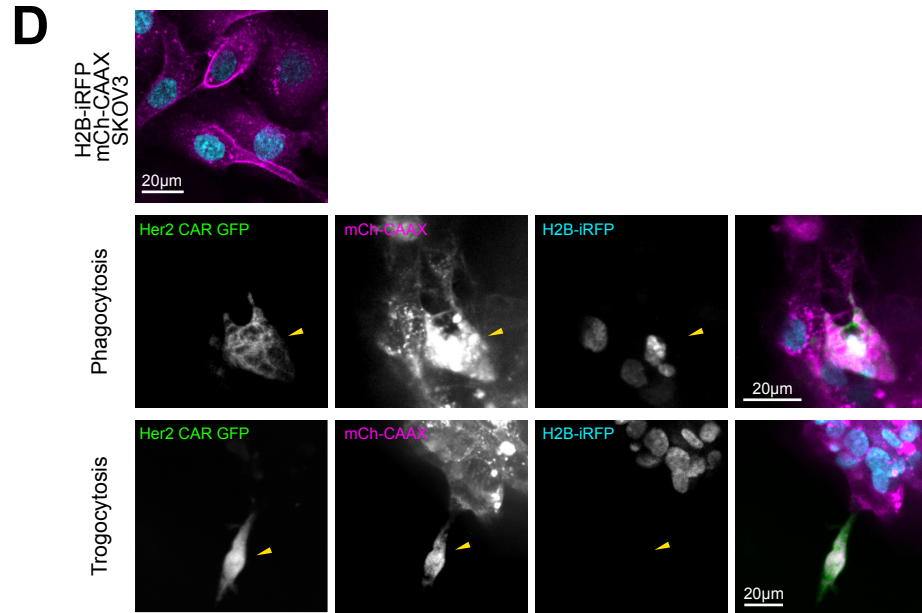
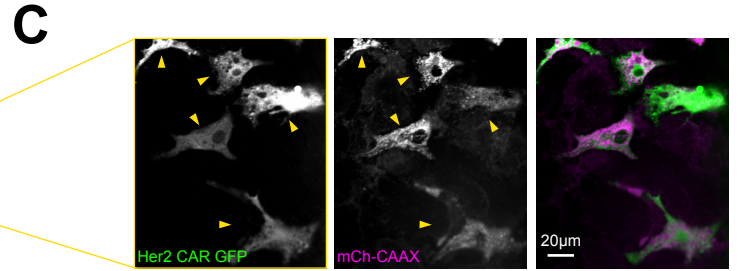
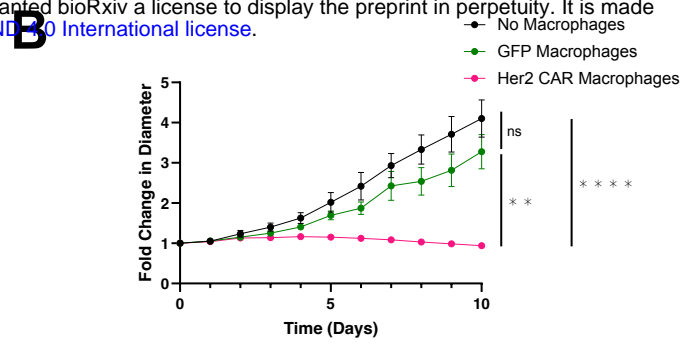
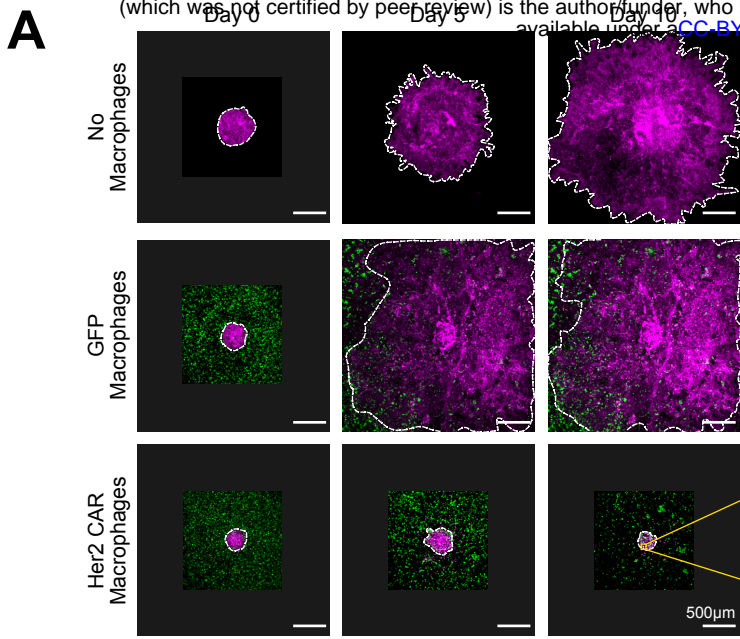


B

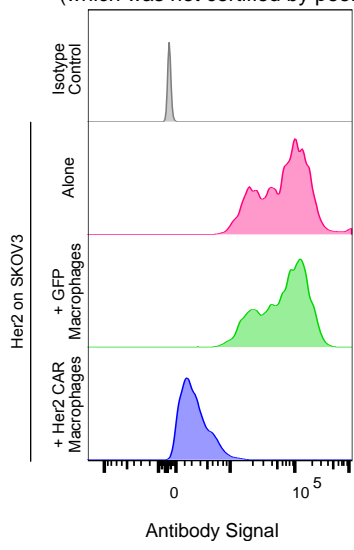


C

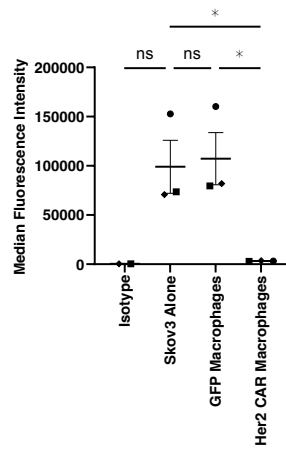




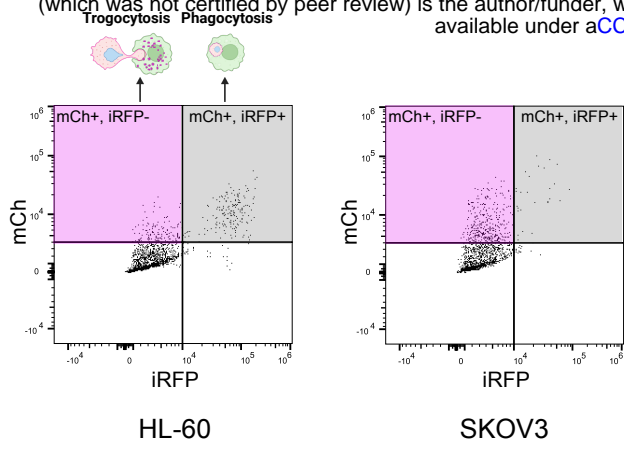
A



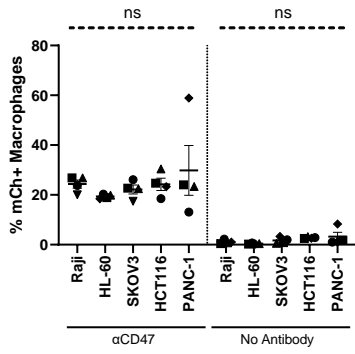
B



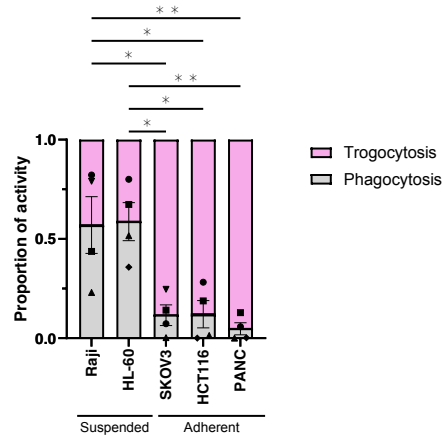
A



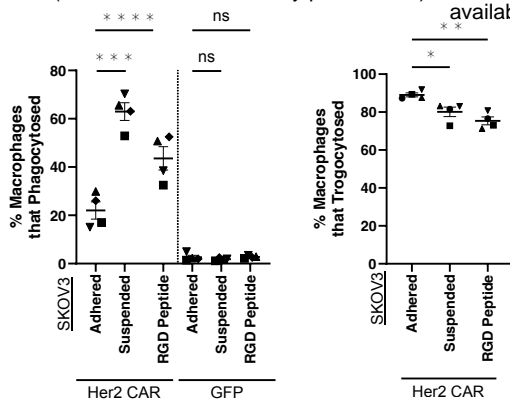
B



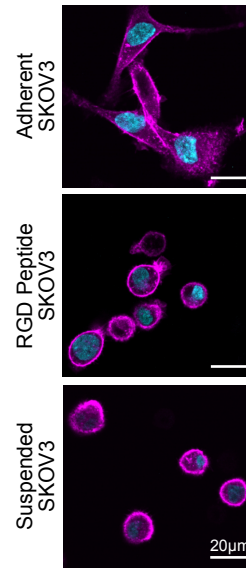
C



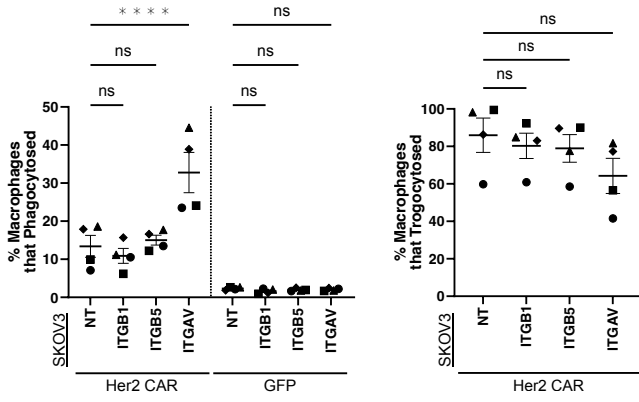
A



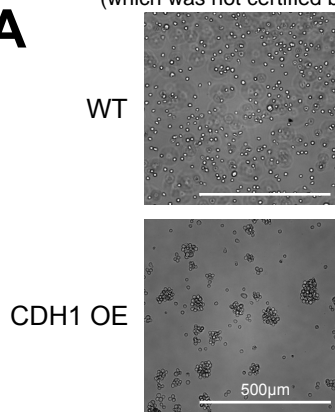
B



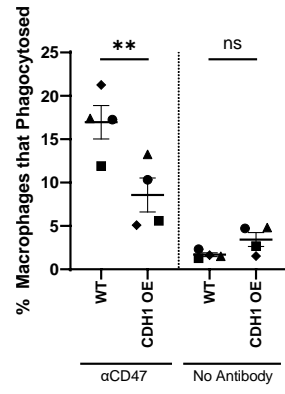
C



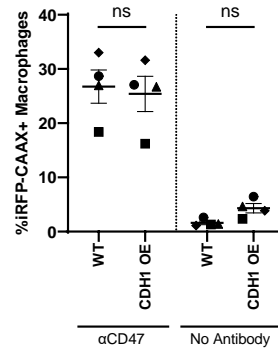
A



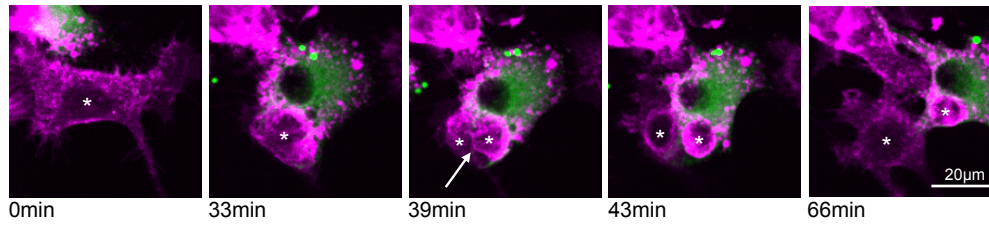
B



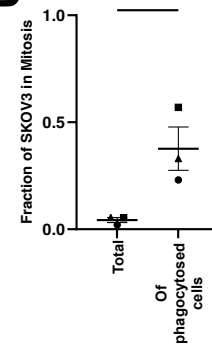
C



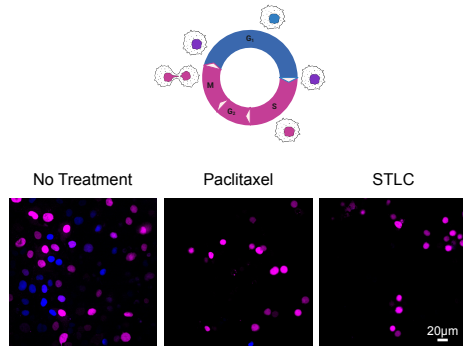
A



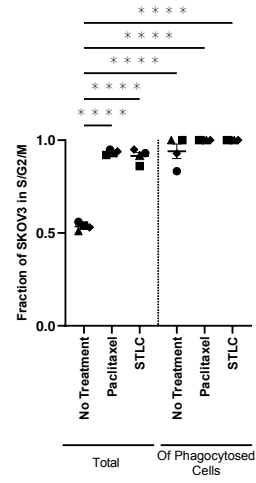
B



C



D



E

